sciendo

LATVIAN JOURNAL OF PHYSICS
AND TECHNICAL SCIENCES
2023, N 6

DOI: 10.2478/lpts-2023-0033

NANOPORE FORMATION AT THE JUNCTIONS OF THE POLYCRYSTAL INTERGRANULAR BOUNDARY UNDER PLASTIC DEFORMATION

Y. Suchikova[1*], S. Kovachov[1], A. Lazarenko[1], I. Bohdanov[1], A. I. Popov[2*]

[1] Berdyansk State Pedagogical University,
71100 Berdyansk, UKRAINE
[2] Institute of Solid State Physics, University of Latvia,
8 Kengaraga Str., Riga, LV-1063, LATVIA
*e-mail: yanasuchikova@gmail.com, popov@latnet.lv

The article is devoted to the study of the mechanism of nanopore formation in the junctions of polycrystal grains under the plastic deformation of a polycrystal due to the conservative sliding of lattice dislocations. A mechanism for the formation of a stress concentrator at the junction of the polycrystal grain boundaries is proposed. The possibility of relaxation of the stress state due to the formation of a junction nanopore is considered in the paper.

Keywords: *Dislocation, grain boundaries, junction, nanopores, polycrystal, stress concentrators.*

1. INTRODUCTION

Porous semiconductors have been attracting the attention of researchers for more than half a century [1], [2]. They are widely used as: materials for solar panels [3], [4], sensors [5], [6], supercapacitors [7], [8]. Recently, interest in such semiconductors has increased due to the prospect of applying a porous layer as a buffer for growing thin films on a single-crystal substrate [9], [10]. Such a layer serves as a "soft cushion", allowing to reduce the stresses resulting from the inconsistency of the crystal lattices [11]. Porous layers are grown on the surface of single-crystal silicon [12], [13]. Thus, it was shown that the electrochemical treatment of single-crystal silicon in a solution of hydrofluoric acid makes it possible to form an array of cylindrical mutually parallel pores [14]. Often, A3B5 group semiconductors (InP, GaAs, GaP) serve as the basis for creating nanoporous layers [15]–[17]. The study [18]

presents a mechanism for the formation of domain pores on the surface of indium phosphide as a result of anode etching of a semiconductor. It is exhibited that the sliding of the pores can be caused by the crystal-lattice orientation of the surface. The authors of the work [19] have demonstrated the possibility of obtaining a developed porous morphology on InP p-type by vapour-phase etching with two halogen acids (HF and HCl). As a result, it was found that halogen acid vapours (especially HCl) affect the thermal properties of the semiconductor. In the research [20], the correlations between the current density of the semiconductors anodizing and the morphological characteristics of the formed nanostructures were investigated. It was concluded that various semiconductors under the same conditions of electrochemical processing demonstrated different pore formation abilities. For the formation of such porous surfaces, as a rule, high-quality single-crystalline material is used [21], [22]. Among the most common methods for forming porous layers are electrochemical etching [23], photoelectrochemical etching [24], and photolithography [25]. All these methods are aimed at artificially creating pores in a homogeneous material [26]. Such modified surfaces and volumes acquire a number of non-standard properties distinguishing porous layers from their crystalline counterparts. First, there is a fundamental increase in the effective surface area, which can be successfully used in photovoltaics (PV) [27]. Secondly, there is a change in the indexes of reflection and absorption of light, which has found its application in photovoltaic energy converters [28]. In addition, the fact of reducing the mass of the crystalline material is interesting and may contribute to the creation of lightweight crystals [29]. In addition to these features, it is also necessary to acknowledge the reduction of internal stresses of the material due to the release of dislocations through an open pore [30], [31].

Apart from the artificial introduction of pores into a crystalline material, a spontaneous pore formation may take place [32], [33]. In particular, pores can form at the junctions of polycrystal grains [34], [35]. This sphere of study is quite interesting from the point of view of using cheaper analogues of porous single crystals. It is commonly known that growing a single crystal with subsequent surface modification is a very high-tech technology requiring huge resources, modern equipment and high costs [36]. Polycrystalline materials are much easier to grow [37]. To optimize the mechanical properties of alloys, grain size and texture are often manipulated by thermomechanical processing, including deformation and annealing [38]. The question of the mechanisms of pore self-organization in the volume of such semiconductors, their concentration and size remains not fully resolved. The proposed study focuses on modelling the process of the appearance of the pores in places of stress concentration at the junctions of the polycrystal grain boundaries.

2. PROBLEM STATEMENT

The main feature of the polycrystal structure in comparison with single crystals and amorphous solids is the presence of two-dimensional defects, namely, grain boundaries. Grain boundaries are the surfaces on which the differences in the orientation of the crystal planes of adjacent single-crystal grains of polycrystals are matched. In most polycrystalline structures, excluding “bamboo” polycrystals, grain boundaries intersect

to form triple junctions (TJs). TJs are linear defects along which the differences of the grain boundaries are consistent.

This alignment occurs mainly due to local transformations or violations of the ideal crystal structure and the redistribution of such dynamic defects as vacancies and dislocations under the influence of various external factors (temperature gradients, force fields, mechanical loads).

One of the most important consequences of the matching processes occurring at the grain boundaries and junctions is the formation of stress concentrators of various types. Among them, we can distinguish concentrators of a diffusive, dislocation, and disclination nature [39], [40]. A dislocation-type concentrator is a dislocation that takes place at the junction of grain boundaries. The junction dislocation is an analogue of the lattice dislocation, but it is considered not as a part of the crystal lattice of an individual grain, but in conditional (virtual) constructs: the lattice of grain boundary shifts, the complete lattice of overlaps, and the lattice of coincident nodes of crystal grains forming the junction [41], [42]. Such concentrators play a defining role in the further evolution of the polycrystal, being responsible for local accommodation processes. In the junctions of the grain boundaries, the processes of plastic deformation of polycrystals are coordinated. If it is impossible to relax the dislocation-type junction stress concentrator, the plastic deformation process slows down or undergoes qualitative changes. The relaxation of the junction concentrator can be carried out due to local accommodation in the near-junction region of the polycrystal, or due to the pore formation.

A dislocation-type concentrator, as a rule, occurs in junctions formed by special grain boundaries as a result of the interaction of dislocations entering the junction along the grain boundaries.

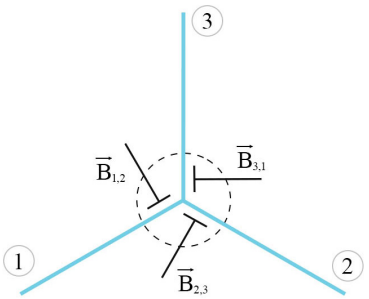

Fig. 1. A model of a junction dislocation with the Burgers vector $\vec{B} = \overrightarrow{B_{1,2}} + \overrightarrow{B_{1,3}} + \overrightarrow{B_{3,2}}$, formed as a result of matching grain boundary shifts $\overrightarrow{B_{1,2}}; \overrightarrow{B_{1,3}}; \overrightarrow{B_{3,2}}$ - Burgers vectors of grain boundary dislocations.

The operating conditions of polycrystalline materials imply the inevitable occurrence of internal stresses, both due to purely mechanical loading and as a result of the influence of temperature gradients and external force fields. Let us consider the most basic case of mechanical loading, which, in general, does not limit the comprehensiveness of the result.

If an external mechanical load is applied to a polycrystal, ensuring that the Peierls barrier is overcome by lattice dislocations (LD), then a conservative movement (sliding) of dislocations becomes possible in the grain volume. Obviously, this sliding is limited by the volume of the grain itself and stops at its boundaries.

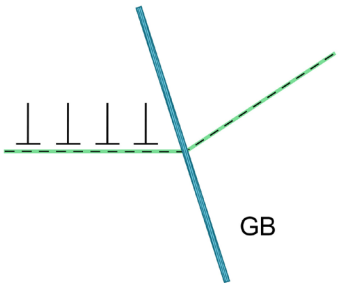

Fig. 2. Formation of a cluster of parallel dislocations inhibited by the boundary of polycrystal grains in the sliding plane.

The lattice dislocation slows down before the grain boundaries and stops moving. However, there might be several LD in this sliding plane meaning that there is a Frank-Reed type dislocation source. It is a segment of the dislocation line, the ends of which are fixed to any obstacles to the conservative sliding of the dislocation, for example, inclusions, complexes of point defects, a grid of dislocations, pores. Under the influence of an external force, the segment continues to slide conservatively, remaining fixed at the ends. As a result, dislocation loops are formed. The peculiarity of the Frank-Reed source is that it is not disposable – after the formation of a loop, it restores its original form and is triggered again. A cluster of identical dislocations (with the same Burgers vectors and the same line directions) is formed in front of the grain boundaries (GB). These dislocations repel each other in the sliding plane. In the equilibrium distribution (stationary position) they are held by an external mechanical load.

The parameters of the equilibrium distribution of dislocations in the continuum approximation depend on the Burgers vector of dislocations, the elastic modules of the sample, and are determined by the dependencies [44]:

$$\rho(\chi) = \frac{\sigma_0}{\pi D}\sqrt{\frac{1-\chi}{\chi}} \; ; \quad l = \frac{2BD}{\sigma_0} \; , \qquad (1)$$

where $\rho(\chi)$ – the linear dislocation density $\rho(\chi)d\chi$ is the sum of the Burgers vectors of dislocations that fall on the linear differential spatial interval $d\chi$;

σ_0 – a flat uniform field of mechanical stresses of external origin caused by an external force (displacement, compression, tension) applied to the outer surface of a polycrystal;

l – the length of the interval of arrangement of clusters of lattice dislocations;

χ – the distance from the grain boundary in the plane of conservative dislocation plane;

B – the sum of the Burgers vectors of all dislocations in the cluster;

$D = \frac{\mu}{2\pi(1-\nu)}$ – an index implemented for the convenience of writing formulas;

μ – the displacement modulus of the sample material;

ν – Poisson's ratio of the sample material.

In this case, before the dislocation, which has gone into the grain boundary, mechanical stresses are concentrated according to the law:

$$\sigma(\chi) = \sigma_0\sqrt{\frac{l}{\chi}} \, . \qquad (2)$$

Given that the distance to the next dislocation is equal to the width of the grain boundary $\chi = \delta$, and using (1) and (2), it becomes possible to estimate the stress concentration directly beyond the grain boundary:

$$\sigma(\delta) = \left(2\sigma_0 D\frac{B}{\delta}\right)^{\frac{1}{2}} \, , \qquad (3)$$

where δ – the width of the grain boundary.

The displacement modulus μ, (respectively, and the index D) far exceed the value of their own mechanical load σ_0. The total Burgers vector of cluster B is at least equal to the width of the grain boundary δ. Accordingly, the stress concentration (3) will be sufficient for the dislocation shift to pass through the boundary into the adjacent grain. In this case, a dislocation of the orientation mismatch (DOM) is formed at the grain boundary (Fig. 3).

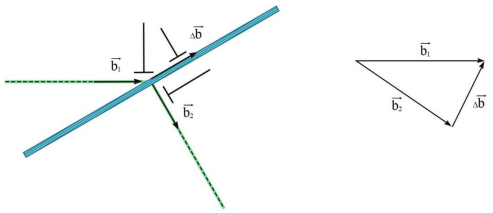

Fig. 3. The scheme of the lattice dislocation passing through the grain boundary with the formation of an orientation mismatch dislocation.

The Burgers vector is determined based on the condition of preserving the total Burgers vector in dislocation reactions:

$$\overline{b}_1 = \overline{b}_2 + \Delta\overline{b}\,;\ \Delta b = \overline{b}_1 - \overline{b}_2\ , \qquad (4)$$

where $\overrightarrow{b_1}$ – the Burgers vector of the LD in the first grain (before passing through the grain boundary);

$\overrightarrow{b_2}$ – the Burgers vector of the LD in the second grain (after passing through the grain boundary);

$\Delta\vec{b}$ – the Burgers vector at the dislocation of the orientation mismatch.

It can be concluded that the concentration of stresses from the accumulation of parallel lattice dislocations, inhibited by the boundary of adjacent grains in the sliding plane, is able to ensure the propagation of the dislocation shift from one grain of a polycrystal to the adjacent one. In this case, the sliding planes of dislocations in adjacent grains should not be parallel. Matching the transition of the lattice dislocation from one sliding plane to another leads to the formation of a grain-boundary dislocation of the orientation mismatch.

3. MECHANISM OF PORE FORMATION IN THIN POLYCRYSTALS

Consider a situation where the structure of the grain boundary is ordered. Also, let us assume that the movement of the dislocation of the orientation mismatch in the grain boundary plane occurs mainly due to sliding. The assumption seems reasonable due to the fact that the propagation of the dislocation shift into the adjacent grain will preferably occur through such a grain boundary, where the rapid departure of the dislocation of the orientation mismatch from the place of agreement of the dislocation shifts will ensure a decrease in the stress concentration.

For a fine-grained polycrystal with a "parquet" structure, the grain boundary can be considered flat. Figure 4 allows determining the directions of the sliding planes in adjacent grains, which provide the possibility of conservative sliding of the dislocation of the orientation mismatch. In this case, the dislocation line and its Burgers vector lie in the grain boundary plane.

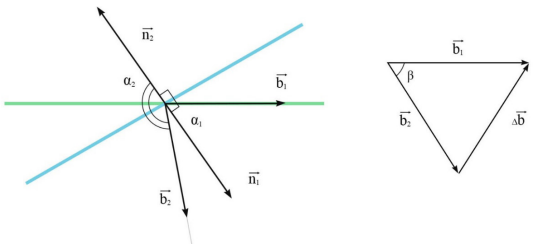

Fig. 4. Scheme for calculating the Burgers vector at dislocation of the orientation mismatch $\Delta\vec{b}$: $\overrightarrow{n_1}$ – unit normal to the grain surface 1; $\overrightarrow{n_2}$ – unit normal to the grain surface 2; α_1 – the angle between the vectors $\vec{b}_1$ and $\overrightarrow{n_1}$; α_1 – the angle between the vectors $\vec{b}_2$ and $\overrightarrow{n_2}$; β – the angle between the vectors $\vec{b}_1$ and $\overrightarrow{b_2}$ i.

Respectively, in Fig. 4, the angle between the Burgers vectors of dislocations in the first and second grain is equal to:

$$\beta = \begin{cases} \pi - (\alpha_2 - \alpha_1), & \text{if } \vec{b}_1 \text{ i } \vec{b}_2 \text{ located on different sides of the normals line;} \\ \pi - (\alpha_2 + \alpha_1), & \text{if } \vec{b}_1 \text{ i } \vec{b}_2 \text{ located on the dislocation of the orientation} \\ & \text{mismatch side of the normals line;} \end{cases} \quad (5)$$

where β – the angle between the vectors $\vec{b}_1$ and $\vec{b}_2$;
α_1 – the angle between the vectors $\vec{b_1}$ and the unit normal to the grain boundary 1;
α_2 – the angle between the vectors $\vec{b_2}$ and the unit normal to the grain boundary 2.

It should be taken into account that the normal has an external direction in relation to the grain volume. It also follows from Fig. 4 that the Burgers vector at dislocation of the orientation mismatch lies in the plane of the grain boundary if the angle between it and the Burgers vector LD of the first grain is equal to $(\pi/2 - a_1)$ or $(\pi/2 + a_1)$. This condition is met if:

$$\cos(\overline{b_1}^{\wedge}, \Delta\bar{b}) = \begin{cases} \cos(\frac{\pi}{2} - \alpha_1) \\ \cos(\frac{\pi}{2} + \alpha_2) \end{cases} = \begin{cases} \sin\alpha_1 \\ -\sin\alpha_1 \end{cases}, \quad (6)$$

$$\cos\beta = \begin{cases} \cos(\pi - (\alpha_2 - \alpha_1)) = -\cos(\alpha_2 - \alpha_1) \\ \cos(\pi - (\alpha_2 + \alpha_1)) = -\cos(\alpha_2 + \alpha_1) \end{cases}, \quad (7)$$

$$\Delta b = (b_1^2 + b_2^2 - 2b_1 b_2 \cos\beta)^{\frac{1}{2}}. \quad (8)$$

The obtained relations (9) are geometric criteria. When one of them is met, the dislocation of the orientation mismatch line and its Burgers vector lie in the grain boundary plane. Such placement will provide the possibility of conservative sliding of the dislocation of the orientation mismatch in the plane of the grain boundary.

A more detailed analysis of the conditions (9) is quite complex. It requires a rigorous description of the crystal structure, along with the use of statistical and probabilistic approaches. However, for a general understanding of the process of matching dislocation shifts in the grain boundary, it is sufficient for each specific set of values of the Burgers vectors and angles to check whether at least one of these equalities is true or not.

As an example of the application of the obtained conditions, we can consider the simplest case when the modules of the Burgers vectors of both lattice dislocations and dislocation of the orientation mismatch coincide. This means that the triangle in Fig. 2 will be equilateral. Then, according

to (7), either the sum or the difference α_1 and α_2 must be equal to $2\pi/3$.

Thus, if the dislocation reaction (4) satisfies one of the equalities (9), a dislocation of the orientation mismatch is formed at the grain boundary, which is capable of conservative movement along the grain boundary.

The dislocation reaction (4), the passage of the LD through the grain boundary, and the formation of the dislocation of the orientation mismatch occur due to the concentration of stresses from the accumulation of parallel LD, inhibited in the same sliding plane in front of the grain boundary. The source that supplies the dislocations for the cluster continues to operate. As a result, the level of stress concentration in the head of the cluster is restored. The dislocation that has passed the grain boundary moves away from it deeper into the volume, and the dislocation of the orientation mismatch moves away from the place of its formation along the grain boundary at their junction.

The dislocation reaction (4) is repeated periodically, and a "torch" of the LD is formed in the adjacent grain, which spreads from the grain boundary. Inside the grain boundary itself, a cluster of dislocation of the orientation mismatch is formed, the movement of which is limited by the triple junction (TJ) of the grain boundary.

The triple junction of the grain boundaries of polycrystals is formed as a result of the intersection of three-grain boundary planes along a specific linear defect - the TJ grain boundary channel. Schematically, the TJ is shown in Fig. 5.

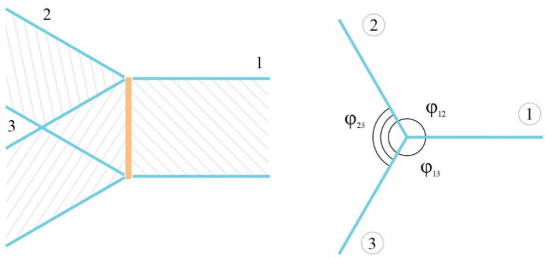

a) b)

Fig. 5. Schematic representation of the triple junction of grain boundaries: a) a spatial view for the case of a "parquet" polycrystal; b) a top view; φ_{12} φ_{13} φ_{23} angles between the grain boundary planes.

When the conditions (8) are met, dislocation of the orientation mismatch appears in the boundaries that form the junction. They can move conservatively along the grain boundary planes. When they reach the TJ, dislocation of the orientation mismatch interacts and forms a junction dislocation. This junction dislocation becomes a stress concentrator as the dislocation of the orientation mismatch accumulates at the grain boundaries.

It is possible that the Burgers vectors do not correspond to the condition:

$$\Delta\overline{b_1} + \Delta\overline{b_2} + \Delta\overline{b_3} = 0\,, \qquad (9)$$

where $\Delta\vec{b_1}$ $\Delta\vec{b_2}$ $\Delta\vec{b_3}$ - the Burgers vectors of dislocation of the orientation mismatch are located in the boundaries 1, 2, 3, respectively.

The vector condition (10) can be written as two scalar conditions (Fig. 3b):

$$\pm\Delta b_1 \pm \Delta b_2 \cos\varphi_{12} \pm \Delta b_3 \cos\varphi_{13} = 0\,;\ \pm\Delta b_2 \sin\varphi_{12} - (\pm\Delta b_3 \sin\varphi_{13}) = 0\,. \qquad (10)$$

The "+" sign before the module of the Burgers vector is selected if this vector is directed to the junction; the "–" sign is selected if the Burgers vector of dislocation of the orientation mismatch is directed from the junction.

Junctions that simultaneously meet the conditions (8) and (9) or (10) manifest themselves as effective dislocation of the orientation mismatch drains. Stress concentrators do not form in them. Junctions of this type could play a special role in the processes of plastic deformation of polycrystals, and a polycrystal with an increased density of junction drains for the dislocation of the orientation mismatch should have plastic properties that differ from the average ones. However, in a natural polycrystal, the relative amount of dislocation of the orientation mismatch of junction drains will be negligible.

From the most general considerations, based on Newton's third law, it can be understood that the maximum level of stress concentration in the junction concentrator cannot exceed the maximum level of concentration in the head of the dislocation cluster, which is inhibited by the grain boundary. When the stress concentration levels in the junction and the head of the dislocation cluster are equalized, the process of dislocation shift passing from grain to grain will stop. The resumption of this process will be possible only after the relaxation of the junction stress concentrator.

The relaxation of the junction concentrator can be carried out due to various mechanisms of local plastic deformation, such as: formation of "torches" of dislocation loops, plastic rotations, local migration, etc. [45].

Let us consider the possibility of relaxation of the junction dislocation concentrator due to the formation of a junction pore.

The components of the stress tensor caused by the junction dislocation concentrator for the case of a "parquet" polycrystal are defined as [44]:

$$\sigma_{\rho\rho} = \sigma_{\varphi\varphi} = -\Delta BD\frac{\sin\varphi}{\rho}\ ;\ \sigma_{\rho\varphi} = \Delta BD\frac{\cos\varphi}{\rho}\ , \qquad (11)$$

where ΔB – Burgers vector of junction dislocation; $D = \dfrac{\mu}{2\pi(1-\nu)}$; μ – shift of material; ν – Poisson's ratio of the substance; (ρ,φ) - polar coordinates with the pole at the grain junction.

The value ΔB it can be estimated using the condition of equality of the stress concentration in the head of the dislocation cluster at the grain boundary and the stress concentration in the junction concentrator using expressions (3) and (11).

$$\frac{\Delta BD}{\delta} \approx \pm\left(2\sigma_0 D\frac{B}{\delta}\right)^{\frac{1}{2}};\ \ \Delta B \approx \pm\left(2\delta B\frac{\sigma_0}{D}\right)^{\frac{1}{2}}. \qquad (12)$$

If we take $l \approx d$, where d is the characteristic grain size of a polycrystal (the case of a fine-grained crystal):

$$B = \frac{1}{2}\frac{\sigma_0}{D} d \,. \tag{13}$$

Substituting (12) in (13) we get:

$$\Delta B \approx \pm \frac{\sigma_0}{D} (\delta d)^{\frac{1}{2}} \,. \tag{14}$$

Substituting (14) in (11) we get:

$$\sigma_{\rho\rho} = \sigma_{\varphi\varphi} \approx \pm \sigma_0 (\delta d)^{\frac{1}{2}} \frac{\sin\varphi}{\rho};$$

$$\sigma_{\rho\varphi} \approx \sigma_0 (\delta d)^{\frac{1}{2}} \frac{\cos\varphi}{\rho}. \tag{15}$$

According to (16), a junction dislocation with a positive Burgers vector ΔB (which corresponds to an excessive extra plane) causes mechanical compression stresses in the direction perpendicular to the grain boundaries. This leads to a negative oversaturation of vacancies in the local areas of grain boundaries near their TJ [46]:

$$c = c_0 \exp\left(\frac{\sigma_{nn}\omega_0}{kT}\right), \tag{16}$$

where $\sigma_{nn} = \sigma_{ik} n_i n_k$ – the normal mechanical stresses at the grain boundaries; σ_{ik} – components of the stress tensor; n_i, n_k – the components of the vector of the external normal to the surface; c_0 – the equilibrium concentration of vacancies in the grain boundary at the absolute temperature T; k – the Boltzmann constant; ω_0 – the vacancy volume.

In the approximation of small loads ($\sigma_0 \ll \mu$):

$$c(\rho,\varphi) = c_0 \left(1 - \frac{\sigma_0 (\delta d)^{\frac{1}{2}} \omega_0}{kT} \frac{\sin\varphi}{\rho}\right). \tag{17}$$

The nonequilibrium distribution of the vacancy concentration will cause a diffuse outflow of the substance from the TJ channel:

$$\frac{\Delta V}{\Delta t} = -I \delta d b^3 \,, \tag{18}$$

where I – the flow of vacancies to the TJ; δ – grain boundary width; d – characteristic grain size of a polycrystal; b^3 –volume of the atom; ΔV– the volume of the substance removed from the TJ channel during the time Δt.

The vacancy flow I is calculated according to the diffusion equation:

$$I = -D_{M3} grad(c), \tag{19}$$

where D_{M3} – the diffusion coefficient across the grain boundaries.

Estimating the gradient of the vacancy concentration as the difference between its values at a distance from the junction and near it, we obtain:

$$I \approx -D_{M3} \frac{1}{d} c_0 \frac{\sigma_0 \omega_0}{kT} \left[\left(\frac{d}{\delta}\right)^{\frac{1}{2}} - \left(\frac{\delta}{d}\right)^{\frac{1}{2}} \right]. \tag{20}$$

Since the width of the grain, boundary δ is much smaller than the characteristic grain size d, and the vacancy size is close to the atomic volume b^3, the expression (20) can be written in a simplified form:

$$\frac{\Delta V}{\Delta t} \approx D_{M3} c_0 b^3 (\delta d)^{\frac{1}{2}} \frac{\sigma_0 b^3}{kT} \,. \tag{21}$$

Thus, diffusive mass transfer across grain boundaries can provide the formation of a junction pore if it provides partial or complete relaxation of the junction concentrator.

Partial relaxation of the junction stress concentrator will occur if the energy associated with the pore is less than the energy of the dislocation concentrator.

The energy of a dislocation concentrator is the energy of its stress fields. It can be estimated by the expression (6), which takes into account the contribution of the energy of the dislocation core:

$$W_D = d\frac{\mu\Delta B^2}{4\pi(1-\nu)}\ln\frac{4d}{\Delta B}. \qquad (22)$$

Given that $D = \frac{\mu}{2\pi(1-\nu)}$, we get:

$$W_D = \frac{\delta(d\sigma_0)^2}{2D}\ln\left(4\frac{D}{\sigma_0}\left(\frac{d}{\delta}\right)^{\frac{1}{2}}\right). \qquad (23)$$

We will estimate the pore energy as a function of its radius. The pore energy consists of the elastic strain energy due to the pore and the surface energy of the pore itself.

The junction pore in the first approximation is a hole in the form of a round cylinder, which leads to a geometric stress concentration in its vicinity. The corresponding components of the stress and strain tensors in solving the plane problem of the theory of elasticity ("parquet" polycrystal) in polar coordinates according to [44] have the form:

$$\sigma_{\rho\rho} = \frac{1}{2}\sigma_0\left(1-\frac{\alpha^2}{\rho^2}\right)+\frac{1}{2}\sigma_0\left(1-4\frac{\alpha^2}{\rho^2}+3\frac{\alpha^4}{\rho^4}\right)\cos 2\varphi,$$

$$\sigma_{\varphi\varphi} = \frac{1}{2}\sigma_0\left(1+\frac{\alpha^2}{\rho^2}\right)-\frac{1}{2}\sigma_0\left(1+3\frac{\alpha^4}{\rho^4}\right)\cos 2\varphi,$$

$$\sigma_{\rho\varphi} = -\frac{1}{2}\sigma_0\left(1+2\frac{\alpha^2}{\rho^2}-3\frac{\alpha^4}{\rho^4}\right)\sin 2\varphi,$$

where a – the radius of the pore.

To obtain the components of the strain tensor, we use the relation:

$$U_{ik} = \frac{1}{9K}\delta_{ik}\sigma_{ll}+\frac{1}{2\mu}\left(\sigma_{ik}-\frac{1}{3}\delta_{ik}\sigma_{ll}\right), \qquad (24)$$

where $\boldsymbol{K}$ – is the all-round compression modulus; $\boldsymbol{\mu}$ is the displacement modulus; $\delta_{ik} = \begin{cases}1, i = k\\ 0, i \neq k\end{cases}$

Using the relation between $\boldsymbol{K}$ and the Lame coefficients $\boldsymbol{\lambda}$, $\boldsymbol{\mu}$, we simplify the expression (24)

$$U_k = \frac{1}{2\mu}\left(\sigma_{ik}-\frac{2-5\nu}{9(1+\nu)}\delta_{ik}\sigma_{ll}\right). \qquad (25)$$

We will find σ_{ll}:

$$\sigma_{ll} = \sigma_{\rho\rho}+\sigma_{\varphi\varphi} = \sigma_0 - 2\sigma_0\frac{a^2}{\rho^2}\cos 2\varphi$$

Then the components of the strain tensor U_{ik}:

$$U_{\rho\rho} = \frac{1}{4}\frac{\sigma_0}{\mu}\left[\frac{5-\nu}{9(1+\nu)}-\frac{\alpha^2}{\rho^2}+\left(1-\frac{4(7+4\nu)}{9(1+\nu)}\frac{\alpha^2}{\rho^2}+3\frac{\alpha^4}{\rho^4}\right)\cos 2\varphi\right],$$

$$U_{\varphi\varphi} = \frac{1}{4}\frac{\sigma_0}{\mu}\left[\frac{5-\nu}{9(1+\nu)} + \frac{\alpha^2}{\rho^2} - \left(1 - \frac{4(2+5\nu)}{9(1+\nu)}\frac{\alpha^2}{\rho^2} + 3\frac{\alpha^4}{\rho^4}\right)\cos 2\varphi\right],$$

$$U_{\rho\varphi} = U_{\varphi\rho} = -\frac{1}{4}\frac{\sigma_0}{\mu}\left(1 + 2\frac{\alpha^2}{\rho^2} - 3\frac{\alpha^4}{\rho^4}\right)\sin 2\varphi. \quad (26)$$

The volume density of the free energy of a deformed body is defined as [44]:

$$F = \frac{\sigma_{ik}u_{ik}}{2}, \quad (27)$$

Here, Einstein's rule of addition over even indices is used.

Substituting (27) and (30) in (31) we get:

$$F = \frac{1}{8}\frac{\sigma^2{}_0}{\mu}\left[1 - \frac{\alpha^2}{\rho^2} + \left(1 - 4\frac{a^2}{\rho^2} + 3\frac{\alpha^4}{\rho^4}\right)\cos 2\varphi\right]\cdot \quad (28)$$

To obtain the energy of the deformed state, it is necessary to calculate the integral:

$$W = d\int_a^d\int_0^{2\pi} F(\rho,\varphi)\rho d\rho d\varphi. \quad (29)$$

Accordingly, all the components of the expression for the free energy density F that have a multiplier of $\cos 2\varphi$, or $\sin 2\varphi$ after integration by $d\varphi$, in the range from 0 to 2π are zeroed. Therefore, to calculate the energy, we can use a much-simplified expression instead:

$$F^{"} = \frac{1}{4}\frac{\sigma_0^2}{\mu}\left[\frac{2(7+4\nu)}{9(1+\nu)} + \frac{55+43\nu}{9(1+\nu)}\frac{\alpha^4}{\rho^4} - 12\frac{\alpha^6}{\rho^6} + 9\frac{\alpha^8}{\rho^8}\right]. \quad (30)$$

Taking $a \approx d$, we simplify:

$$W_1 = \frac{\pi}{2}\frac{\sigma_0^2}{\mu}d\frac{7+4\nu}{9(1+\nu)}\left(d^2 + a^2\right). \quad (31)$$

The surface energy of the pore can be calculated as:

$$W_2 = \gamma S, \quad (32)$$

where γ – the surface energy density; S – the free surface area of the junction pore $S = 2\pi ad$.

Accordingly, to [47] $\gamma \approx 0{,}1\mu b$. Then we get: $W_2 \approx 0{,}2\mu\pi abd$

Thus, the excess energy of the polycrystal associated with the occurrence of the junction pore is estimated as:

$$W_{\check{I}} = W_1 + W_2,$$

$$W_{\check{I}} = 0{,}2\mu\pi abd\left[1 + \frac{\sigma_0^2}{\mu^2}\frac{d}{b}\frac{7+4\nu}{3{,}6(1+\nu)}\left(\frac{d}{a} + \frac{a}{d}\right)\right]. \quad (33)$$

Comparing (26) and (39), we obtain a criterion for the occurrence of a junction pore instead of a dislocation-type junction stress concentrator, as a condition for reducing the energy of the deformed state:

$$W_{\ddot{I}} < W_{\ddot{A}},$$

$$0,2\mu\pi abd\left[1+\frac{\sigma_0^2}{\mu^2}\frac{d}{b}\frac{7+4\nu}{3,6(1+\nu)}\left(\frac{d}{a}+\frac{a}{d}\right)\right]<\frac{\delta(d\sigma_0)^2}{2D}\ln\left[4\frac{D}{\sigma_0}\left(\frac{d}{\delta}\right)^{\frac{1}{2}}\right],$$

given that $D=\frac{\mu}{2\pi(1-\nu)}$:

$$a\left[1+\frac{\sigma_0^2}{\mu^2}\frac{d}{b}\frac{7+4\nu}{3,6(1+\nu)}\left(\frac{d}{a}+\frac{a}{d}\right)\right]<5(1-\nu)\delta\frac{d}{b}\frac{\sigma_0^2}{\mu^2}\ln\left[\frac{2}{\pi(1-\nu)}\frac{\mu}{\sigma_0}\left(\frac{d}{\delta}\right)^{\frac{1}{2}}\right]. \quad (34)$$

For the case of $\left(\frac{\sigma_0}{\mu}\right)^2\frac{d}{ab}\approx 1$, the gap resulting from the relaxation of a dislocation-type junction stress concentrator cannot exceed a certain critical size, which, in the continuum approximation, corresponds to its geometric radius:

$$a_{\hat{e}\delta}=5(1-\nu)\delta\frac{d}{b}\left(\frac{\sigma_0}{\mu}\right)^2\ln\left[\frac{2}{\pi(1-\nu)}\frac{\mu}{\sigma_0}\left(\frac{d}{\delta}\right)^{\frac{1}{2}}\right]. \quad (35)$$

The order of magnitude of the critical pore size is determined by the factor of the natural logarithm. Significant parameters for it are the size of the crystal grain of the polycrystal d, and the modulus of external mechanical stress σ_0. In general, the critical size exceeds the width of the grain boundary by one or two orders of magnitude.

The results obtained evoke ideas about the significance of stress concentrators in general, and junction stress concentrators, in particular, for the processes of plastic deformation of polycrystals. The described mechanism of formation of a junction pore can be used both for determining the optimal parameters for the use of polycrystalline samples and for designing polycrystalline materials and structures with specified properties. It should be noted that the application of the obtained results is limited to the case of fine-grained polycrystals with a "parquet" structure.

The prospects for further research suggest an in-depth study of the energy criteria of the process of matching dislocation shifts in the grain boundary, clarification of the diffusion mechanism of the formation of the junction pore, and extension of the result to the case of a three-dimensional polycrystal.

4. CONCLUSIONS

1. The article describes the mechanism of nanopore formation at the junction of the grain boundaries of a polycrystal with a "parquet structure". At the same time, the following stages of the complete process are studied: formation of a cluster of parallel lattice dislocations inhibited in their sliding plane by the polycrystal grain boundary; passage of a dislocation shift through the grain boundary with the formation of a grain boundary dislocation of an orientation mismatch; coordination of grain boundary shifts at the junction of polycrystal grains with the formation of a junction stress concentrator; relaxation of the stress state of the junction stress concentrator due to the formation of a junction nanopore.
2. A ratio is obtained that allows us to estimate the characteristic size of the nanopore depending on the characteristic grain size of the polycrystal and the value of the external force load.
3. Modeling of the processes leading to the formation of a junction nanopore is carried out in the continuum approximation, which takes into account the variety of possible misorientation of adjacent polycrystal grains.
4. Understanding and detailing the mechanism of the origin and formation of the junction pore will allow you to anticipate, eliminate, or implement this possibility in the processes, including technological ones, associated with the study and operation of polycrystals.

ACKNOWLEDGEMENTS

The study has been supported by the Ministry of Education and Science of Ukraine via Project No. 0122U000129 "The search for optimal conditions for nanostructure synthesis on the surface of A3B5, A2B6 semiconductors and silicon for photonics and solar energy", Project No. 0121U10942 "Theoretical and methodological bases of system fundamentalization of the future nanomaterials experts training for productive professional activity", and Project No. 0123U100110 "System of remote and mixed specialized training of future nanoengineers for the development of new dual-purpose nanomaterials". In addition, the research of A.I.P. and Y.S. has been partly supported by COST Action CA20129 "Multiscale irradiation and chemistry driven processes and related technologies" (MultiChem). A.I.P. thanks the Institute of Solid-State Physics, University of Latvia, ISSP UL as the Centre of Excellence, supported through the Framework Program for European Universities, Union Horizon 2020, H2020-WIDESPREAD-01–2016–2017-TeamingPhase2, under Grant Agreement No. 739508, CAMART2 project.

REFERENCES

1. Chazalviel, J. N., Wehrspohn, R. B., & Ozanam, F. (2000). Electrochemical Preparation of Porous Semiconductors: From Phenomenology to Understanding. *Materials Science and Engineering: B*, *69*, 1–10. doi: 10.1016/S0921-5107(99)00285-8

2. Bellet, D., & Canham, L. (1998). Controlled Drying: The Key to Better Quality Porous Semiconductors. *Advanced Materials*, *10* (6), 487–490.
3. Zhang, M., Cui, X., Wang, Y., Wang, B., Ye, M., Wang, W., ... & Lin, Z. (2020). Simple Route to Interconnected, Hierarchically Structured, Porous Zn2SnO4 Nanospheres as Electron Transport Layer for Efficient Perovskite Solar Cells. *Nano Energy, 71*, 104620. doi:/10.1016/j.nanoen.2020.104620
4. Zhang, X., Wang, B., Huang, L., Huang, W., Wang, Z., Zhu, W., ... & Marks, T. J. (2020). Breath Figure–Derived Porous Semiconducting Films for Organic Electronics. *Science Advances*, *6* (13), eaaz1042. doi: 10.1126/sciadv.aaz1042
5. Zhou, X., Cheng, X., Zhu, Y., Elzatahry, A. A., Alghamdi, A., Deng, Y., & Zhao, D. (2018). Ordered Porous Metal Oxide Semiconductors for Gas Sensing. *Chinese Chemical Letters*, *29* (3), 405–416. doi: 10.1016/j.cclet.2017.06.021
6. Naderi, N., & Moghaddam, M. (2020). Ultra-sensitive UV Sensors Based on Porous Silicon Carbide Thin Films on Silicon Substrate. *Ceramics International*, *46* (9), 13821–13826. doi: 10.1016/j.ceramint.2020.02.173
7. Cai, J., Lv, C., Hu, C., Luo, J., Liu, S., Song, J., ... & Watanabe, A. (2020). Laser Direct Writing of Heteroatom-Doped Porous Carbon for High-Performance Micro-Supercapacitors. *Energy Storage Materials*, *25*, 404–415. doi: 10.1016/j.ensm.2019.10.001
8. Vambol, S., Vambol, V., Suchikova, Y., & Deyneko, N. (2017) Analysis of the Ways to Provide Ecological Safety for the Products of Nanotechnologies throughout their Life Cycle. *Eastern-European Journal of Enterprise Technologies*, *1* (10–85), 27–3. doi 10.15587/1729-4061.2017.85847
9. Ramesh, C., Tyagi, P., Bhattacharyya, B., Husale, S., Maurya, K. K., Kumar, M. S., & Kushvaha, S. S. (2019). Laser Molecular Beam Epitaxy Growth of Porous GaN Nanocolumn and Nanowall Network on Sapphire (0001) for High Responsivity Ultraviolet Photodetectors. *Journal of Alloys and Compounds*, *770*, 572–581. doi: 10.1016/j.jallcom.2018.08.149
10. Gemmel, C., Hensen, J., Kajari-Schröder, S., & Brendel, R. (2017). 4.5 ms Effective Carrier Lifetime in Kerfless Epitaxial Silicon Wafers from the Porous Silicon Process. *IEEE Journal of Photovoltaics, 7* (2), 430–436. doi: /10.1109/JPHOTOV.2016.2642640
11. Suchikova, J.A. (2015). Synthesis of Indium Nitride Epitaxial Layers on a Substrate of Porous Indium Phosphide. *Journal of Nano- and Electronic Physics, 7* (3), 03017.
12. Sundarapura, P., Zhang, X. M., Yogai, R., Murakami, K., Fave, A., & Ihara, M. (2021). Nanostructure of Porous Si and Anodic SiO2 Surface Passivation for Improved Efficiency Porous Si Solar Cells. *Nanomaterials*, *11* (2), 459. doi:10.3390/nano11020459
13. Huang, X., Cen, D., Wei, R., Fan, H., & Bao, Z. (2019). Synthesis of Porous Si/C Composite Nanosheets from Vermiculite with a Hierarchical Structure as a High-Performance Anode for Lithium-Ion Battery. *ACS Applied Materials & Interfaces*, *11* (30), 26854–26862. doi: 10.1021/acsami.9b06976
14. Suchikova, Y. (2016) Provision of Environmental Safety through the Use of Porous Semiconductors for Solar Energy Sector. *Eastern-European Journal of Enterprise Technologies,* 6(5 (84), 26–33. https://doi.org/10.15587/1729-4061.2016.85848
15. Kou, X., Machness, A., Paluch, E., & Goorsky, M. (2018). Homoepitaxial Growth of InP on Electrochemical Etched Porous InP Surface. *ECS Journal of Solid State Science and Technology*, *7* (5), P269. doi/10.1149/2.0161805jss
16. Suchikova, J.A., Kidalov, V.V., & Sukach, G.A. (2009). Blue Shift of Photoluminescence Spectrum of Porous InP. *ECS Transactions*, *25* (24), 59–64. doi: 10.1149/1.3316113
17. Suchikova, Y.A., Kidalov, V.V., & Sukach, G.A. (2010). Influence of the Carrier Concentration of Indium Phosphide on the Porous Layer Formation. *Journal of Nano- and Electronic Physics*, *2* (4), 75–81.

18. Quill, N., Clancy, I., Nakahara, S., Belochapkine, S., O'Dwyer, C., Buckley, D. N., & Lynch, R. P. (2017). Process of Formation of Porous Layers in n-InP. *ECS Transactions,* 77 (4), 67. doi: /10.1149/07704.0067ecst

19. Hassen, M., Kallel, N., & Ezzaouia, H. (2019). Analysis of Morphological, Optical and Thermal Properties of Porous p-Type Indium Phosphide p-InP (100) Prepared by the Vapor Etching Method. *The European Physical Journal Plus*, *134* (7), 1–10. doi: 10.1140/epjp/i2019-12720-1

20. Sychikova, Y.O., Bogdanov, I.T., & Kovachov, S.S. (2019). Influence of Current Density of Anodizing on the Geometric Characteristics of Nanostructures Synthesized on the Surface of Semiconductors of A3B5 Group and Silicon. *Functional Materials, 27* (1), 29–34. doi:10.15407/fm27.01.29

21. Takizawa, T. T. T., Arai, S. A. S., & Nakahara, M. N. M. (1994). Fabrication of Vertical and Uniform-Size Porous InP Structure by Electrochemical Anodization. *Japanese Journal of Applied Physics, 33* (5A), L643. doi: 10.1143/JJAP.33.L643

22. Yana, S. (2016). Porous indium phosphide: Preparation and properties. In Yana, S. *Handbook of Nanoelectrochemistry: Electrochemical Synthesis Methods, Properties, and Characterization Techniques* (pp. 283–306 X). doi: 10.1007/978-3-319-15266-0_9

23. Yang, X., Xi, F., Chen, X., Li, S., Wan, X., Ma, W., ... & Chang, Y. (2021). Porous Silicon Fabrication and Surface Cracking Behavior Research Based on Anodic Electrochemical Etching. *Fuel Cells*, *21* (1), 52–57. DOI:10.1002/fuce.202000048

24. Suohikova, Y., Vambol, S., Vambol, V., Mozaffari, N., & Mozaffari, N. (2019) Justification of the Most Rational Method for the Nanostructures Synthesis on the Semiconductors Surface. *Journal of Achievements in Materials and Manufacturing Engineering*, *92* (1–2), 19–28. doi:10.5604/01.3001.0013.3184

25. Azuelos, P., Girault, P., Lorrain, N., Poffo, L., Guendouz, M., Thual, M., ... & Charrier, J. (2017). High Sensitivity Optical Biosensor Based on Polymer Materials and Using the Vernier Effect. *Optics Express*, *25* (24), 30799–30806. doi:10.1016/j.optmat.2017.07.005

26. Adams, K. J., DeBord, J. D., & Fernandez-Lima, F. (2018). Discovery and Targeted Monitoring of Biomarkers Using Liquid Chromatography, Ion Mobility Spectrometry, and Mass Spectrometry. *Vacuum Science & Technology B, Nanotechnology and Microelectronics: Materials, Processing, Measurement, and Phenomena, 34* (5), 051804, 91. doi:10.1116/6.0000203

27. Niu, J., Albero, J., Atienzar, P., & García, H. (2020). Porous Single-Crystal-Based Inorganic Semiconductor Photocatalysts for Energy Production and Environmental Remediation: Preparation, Modification, and Applications. *Advanced Functional Materials*, *30* (15), 1908984. doi: 10.1109/JPHOTOV.2019.2912069

28. Jafarov, M. A., Nasirov, E. F., Jahangirova, S. A., & Mammadov, R. (2019). Nanostructured Cu2ZnSnS4 Thin Films on Porous-Si Wafer. *Journal of Materials and Applications*, *8* (1), 28–33. doi:10.1134/S1063785019020342

29. Heinke, L., & Wöll, C. (2019). Surface-Mounted Metal–Organic Frameworks: Crystalline and Porous Molecular Assemblies for Fundamental Insights and Advanced Applications. *Advanced Materials*, *31* (26), 1806324. doi:10.1002/adma.201806324

30. Suchikova, Y.A., Kidalov, V.V., & Sukach, G.A. (2011). Influence of Dislocations on the Process of Pore Formation in n-InP (111) Single Crystals. *Semiconductors*, *45*, 121–124. doi:10.1134/S1063782611010192

31. Zimin, S., Vasin, V., Gorlachev, E., Naumov, V., Petrakov, A., & Shilov, S. (2011). Fabrication and Study of Porous PbTe Layers on Silicon Substrates. *Physica Status Solidi C*, *8* (6), 1801–1804. doi: 10.1002/pssc.201000025

32. Ulin, V. P., & Konnikov, S. G. (2007). Electrochemical Pore Formation Mechanism in III–V Crystals (Part I). *Semiconductors*, *41*, 832–844. doi:10.1134/S1063782607070111

33. Guarini, K. W., Black, C. T., Milkove, K. R., & Sandstrom, R. L. (2001). Nanoscale Patterning Using Self-Assembled Polymers for Semiconductor Applications. *Journal of Vacuum Science & Technology B: Microelectronics and Nanometer Structures Processing, Measurement, and Phenomena*, *19* (6), 2784–2788. doi: 10.1116/1.1421551
34. Rehn, V., Hötzer, J., Rheinheimer, W., Seiz, M., Serr, C., & Nestler, B. (2019). Phase-field Study of Grain Growth in Porous Polycrystals. *Acta Materialia*, *174*, 439–449. doi:10.1016/j.actamat.2019.05.059
35. Tikare, V., Miodownik, M. A., & Holm, E. A. (2001). Three-Dimensional Simulation of Grain Growth in the Presence of Mobile Pores. *Journal of the American Ceramic Society*, *84* (6), 1379–1385. doi:10.1111/j.1151-2916.2001.tb00845.x
36. Chen, C., Sun, S., Chou, M., & Xie, K. (2017). In situ Inward Epitaxial Growth of Bulk Macroporous Single Crystals. *Nature communications*, *8* (1), 1–8. doi:10.1038/s41467-017-02197-6
37. Ng, K. W., Ko, W. S., Chen, R., Tran, T. T. D., Lu, F., Chuang, L. C., ... & Chang-Hasnain, C. (2010). Nanolasers grown on polycrystalline silicon. In *2010 23rd Annual Meeting of the IEEE Photonics Society* (pp. 78-79). IEEE. doi:10.1109/PHOTONICS.2010.5698766
38. McDonald, S. A., Burnett, T. L., Donoghue, J., Gueninchault, N., Bale, H., Holzner, C., ... & Withers, P. J. (2021). Tracking Polycrystal Evolution Non-destructively in 3D by Laboratory X-ray Diffraction Contrast Tomography. *Materials Characterization*, *172*, 110814. doi: 10.1016/j.matchar.2020.110814
39. Lazarenko, A. S., Mikhailovskij, I. M., Rabukhin, V. B., & Velikodnaya, O. A. (1995). Nanotopography and Grain-Boundary Migration in the Vicinity of Triple Junctions. *Acta metallurgica et materialia*, 43 (2), 639–643. doi:10.1016/0956-7151(94)00228-A
40. Lazarenko, A.S., Rabukhin, V.B., & Slezov, V.V. (1991). Concerning the Formation of a Junction Disclination at a Triple Junction of Boundaries under Conditions of Low-Temperature Diffusion Creep. *Physics of Metals and Metallography*, *72* (3), 48.
41. Perevezentsev, V. N., Kirikov, S. V., & Svirina, Y. V. (2020). Conditions of Strain-Induced Facet Formation during Interaction between a Lattice Dislocation Pile-Up and a Grain Boundary. *Physics of Metals and Metallography, 121*, 935 doi: 10.1134/S0031918X20100087
42. Kirikov, S.V., & Perevezentsev, V.N. (2021). Analysis of the Conditions for the Existence of Stable Microcracks in an Elastic Stress Field from a Rotational-Shear Mesodefect. *Letters on Materials, 11* (1), 50–54. doi: 10.22226/2410-3535-2021-1-50-54
43. Perevezentsev, V. N., & Chuvil'deev, V. N. (1992). The Theory of Structural Superplasticity—II. Accumulation of Defects on the Intergranular and Interphase Boundaries. Accommodation of the Grain-Boundary Sliding. The Upper Bound of the Superplastic Strain Rate. *Acta metallurgica et materialia*, *40* (5), 895–905. doi:10.1016/0956-7151(92)90066-N
44. Landau, L. D., & Lifshitz, E. M. (2013). *Quantum mechanics: Non-relativistic theory* (Vol. 3). Elsevier.